# Calculating Vacuum Metal Infiltration Rate and Depth of BN-Al Composite Materials

Chao Wang[1]*, Zhefu Li[2], Mengge Dong[3], Lu Zhang[4], Jianxing Liu[3], Xiaozhou Cao[3], and Xiangxin Xue[3]*

[1]Department of Mechanical Engineering, The University of Texas at Dallas, Richardson, TX, 75080, USA
[2]Shanghai Synchrotron Radiation Facility (SSRF), Shanghai Advanced Research Institute, Chinese Aacademy of Sciences, Shanghai, 201204, China
[3]School of Metallurgy, Northeastern University, Shenyang, Liaoning, 110819, China
[4]School of Energy and Environment, Anhui University of Technology, Ma'anshan, 243002, China

Chao Wang, Zhefu Li, and Mengge Dong made an equal contribution.

*Corresponding author. E-mail: wang.chao@utdallas.edu, xuexx@mail.neu.edu.cn

**Abstract**

Although ceramic-metal composite materials prepared by a metal infiltration process have spurred a a great deal of recent research, the calculation of the metal infiltration rate and infiltration depth has not been as intensely studied. This article is the first to conduct calculations and research on the metal infiltration of BN-Al composites. When the metal infiltration temperature is 1100 °C and the infiltration time is 7200 s, the final infiltration depth can reach 0.21 m. When the time is increased, the rate gradually decreases. When the metal infiltration was first started, the maximum infiltration rate was 0.65 cm·min$^{-1}$, and when the metal infiltration was completed, the infiltration rate had dropped to 0.18 cm·min$^{-1}$.

**Keywords**: Vacuum infiltration, BN-Al, Infiltration rate, Infiltration depth, Composite material

## Introduction

Boride ceramic is a new type of material with many important properties (1-4). These include a high melting point, great hardness, high chemical stability, high wear resistance, and corrosion resistance (5-8). As a result of these characteristics, it can be used as a refractory material and in the production of engineering ceramics and has many applications in areas such as aerospace and the nuclear industry (9-14).

Its great weakness, however, is its brittleness. Under stress, cracks can occur, and worse, fractures can lead to material failure (15-18). The use of high-strength, high-purity metal and matrix composites is an effective method of improving ceramic insulation and reliability (18-20).

Ceramic-metal composite material, also known as cermet, is a new type of material that can enhance transportation capacity and energy conversion (21-23). Cermet combines the main advantages of ceramics and metals, including the high temperature stability of ceramics, and the workability and ductility of metals (24-27).

The use of metal infiltration (Melt Infiltration) is the first step in the preform phase (28-30). Melted metal is poured into the preform, and through a combination of capillary action and the application of a certain amount of pressure, the molten metal is impregnated into the gap of the preform, creating the composite material which combines metal with ceramic (Figure 1).

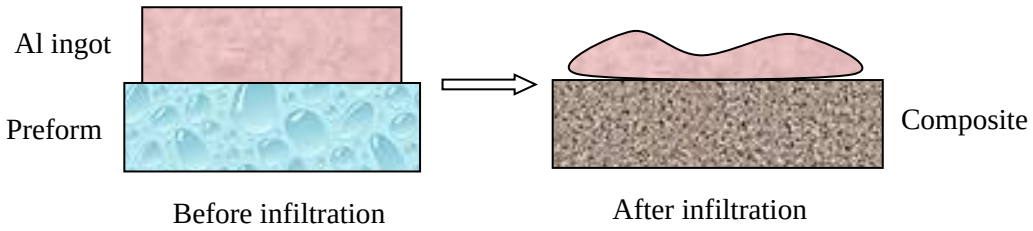


**Figure 1** Schematic diagram of melt infiltration

## Principle of metal infiltration

The principle of metal infiltration is based on the knowledge that preform is a porous medium, and the flow of liquid metal in this porous medium can be compared to the flow in a capillary bundle with a certain equivalent diameter. Capillary pressure ( $P_c$ ) is the additional pressure caused by the surface tension between the front part of the liquid flow and the gas. From the perspective of statics, the additional pressure caused by capillary action determines whether the seepage process is automatically carried out (31). The capillary pressure is determined by the Laplace equation:

$$P_c = 2\sigma \cos\theta / r \tag{1}$$

in which, $\sigma$ is liquid-gas surface tension, $\theta$ is wetting angle between liquid metal and particles, $r$ is hydraulic radius.

$$r = d_p\phi / 6(1-\phi) \tag{2}$$

in which, $d_p$ is the particle radius, $\phi$ is the apparent porosity of the preform.

$$\phi = \frac{V_1}{V_2} \tag{3}$$

in which, $V_1$ is the interstitial volume of preform, and $V_2$ is the total volume occupied by preforms.

Regarding equation (1): When $\theta < 90^\circ$ and $P_c > 0$, metal infiltration can be carried out automatically. When $\theta > 90^\circ$ and $P_c < 0$, metal infiltration cannot be performed automatically. In addition, for the molten metal to penetrate forward through the gap of the preform, the molten metal should have the wetting property of the particle surface.

## Calculation of metal infiltration

In performing metal infiltration, time, pore size, pore shape, apparent porosity, metal viscosity and surface tension of the molten metal have a great impact on the kinetics of metal infiltration. Consequently, metal infiltration is calculated based on these factors. The depth of penetration into the preform is of great importance in judging whether the metal infiltration has been successfully completed.

The formula for calculating the depth of metal infiltration is:

$$h = \left[ t\left( \frac{\varepsilon_p}{1-\varepsilon_p} \right) \frac{r\lambda\gamma}{6.25\mu} \cos\theta \right]^{1/2} \tag{4}$$

in which $h$ is the depth of infiltration, $r$ is the particle radius (5 μm is applied in this calculation), $\lambda$ is the pore shape factor (in this calculation, 0.75), $\gamma$ is the surface tension, $\mu$ is the metal viscosity, $\varepsilon$ is the porosity of the preform (using the average value of apparent porosity of 0.375 in this calculation), $\theta$ is the wetting angle, $t$ is the metal infiltration time.

Fujii studied the wettability of hexagonal BN and Al, and the results showed that 1373 K (1100 °C) is the best temperature for Al infiltration of BN (32).

The viscosity of metallic aluminum at 1100 °C can be calculated using the equation (2), and the calculation result is $\mu$ =0.903 mPa·s;

$$\mu = 0.1492 \exp(1984.5/T)[mPa{\cdot}s] \tag{2}$$

The surface tension of metallic aluminum at 1100 °C can be obtained using equation (3), where T is the metal infiltration temperature of 1100 °C, the melting temperature of metallic aluminum is 660 °C, and the calculated result is: $\gamma$ =0.80 J·m$^{-2}$;

$$\gamma = 0.868 - 0.152(T - T_m) \times 10^{-3}[J/m^2] \tag{3}$$

Fujii also measured and drew the wetting angle curve between BN and Al (Figure 2). When the temperature is 1173K (900 °C) and the wetting time is 3500 seconds (s), the wetting angle is greater than 120 °C. When the temperature is 1273K (1000 °C), and the wetting time is 7000~7500 seconds (s), the wetting angle will decrease to 0°. When the temperature is 1373K (1100 °C) and the wetting time is 2000~2500 seconds (s), the wetting angle will decrease to 0°. Fujii's research has shown that 1373K (1100 °C) is the best temperature for Al infiltration of BN.

The wetting angle at 1100 °C is calculated in Figure 2:

$$\theta = 29.14 - 0.01t(500s < t < 2500s) \tag{4}$$

$$\theta = 0(t > 2500s) \tag{5}$$

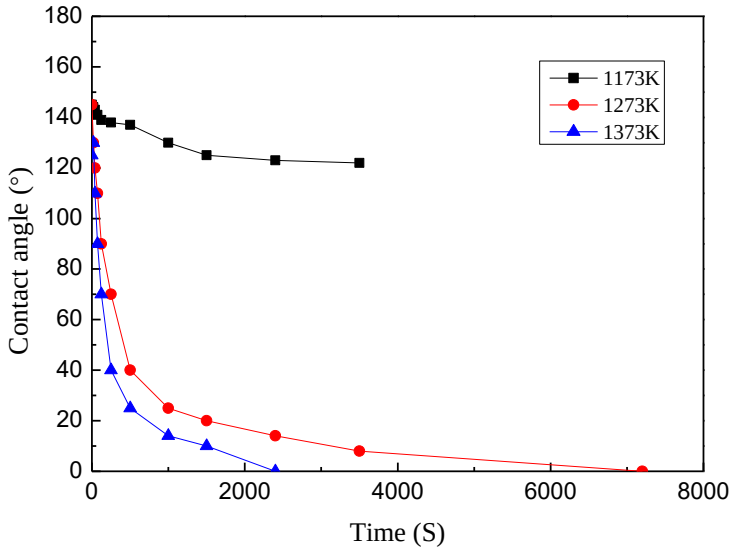


**Figure 2** Contact angle curves between Al and BN (32)

Based on the above calculation, the relationship between metal infiltration depth and the time of the BN-based boron-containing composite material is obtained using the following equation:

$$h = \sqrt{0.0000064t\cos(29.14 - 0.01t)}(500s < t < 2500s)[m] \quad (6)$$

$$h = \sqrt{0.0000064t}(t > 2500s)[m] \quad (7)$$

According to the above calculation of the infiltration depth, time is the abscissa, and the depth is the ordinate. Figure 3 shows the relationship between metal infiltration depth and time of the BN-based, boron-containing composite materials. It can be seen from the figures that as time increases, the infiltration depth gradually increases. When the infiltration time is 7200 s, the final infiltration depth can reach 0.21 m. This outcome indicates that the sample thickness of the preform prepared in the laboratory must be less than 0.21 m to ensure final completion of the metal infiltration.

Determining the data of infiltration depth $h$ and time $t$:

$$h = 0.0384 + 2.93\times10^{-5}t - 2.12\times10^{-9}t^2(R^2 = 0.99642) \quad (8)$$

The metal infiltration rate $v$ is calculated by equations (7) and (8), and demonstrate the relationship between the infiltration rate $v$ and time $t$:

$$v = \frac{h}{t} = \sqrt{\frac{0.0000064\cos(29.14 - 0.01t)}{t}}(500s < t < 2500s)[m/s] \quad (9)$$

$$v = \frac{h}{t} = \sqrt{\frac{0.0000064}{t}} (t > 2500s)[m/s] \tag{10}$$

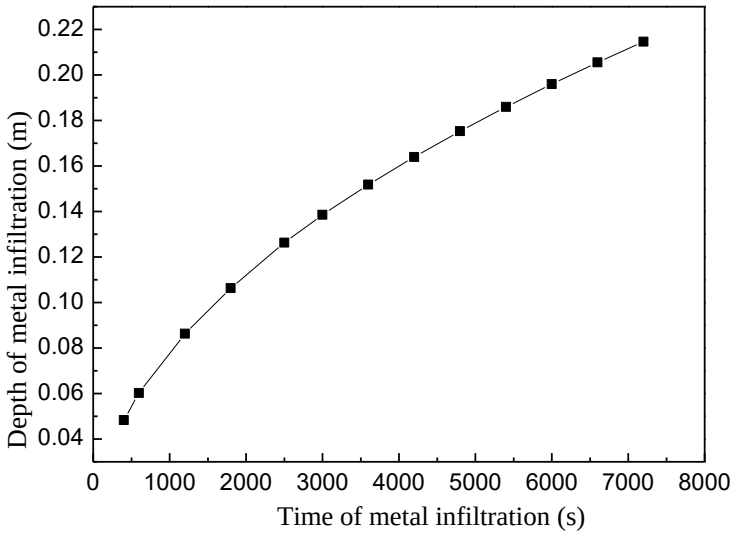


**Figure 3** The relationship between depth and time of infiltration

Based on the above calculation of the infiltration rate, the time is the abscissa, and the velocity is the ordinate for drawing. Figure 4 shows the relationship between the metal infiltration rate and time of TiB2-based composites. It can be seen from the figure that as time increases, the metal infiltration rate gradually decreases. When the metal infiltration is just beginning, the maximum infiltration rate is 0.65cm·min$^{-1}$. When the metal infiltration is over, the infiltration rate has dropped to 0.18cm·min$^{-1}$. This outcome indicates that the rate of metal infiltration has not been consistent during the infiltration process. The reason for the gradual decrease is probably because the pores of the preform have been gradually filled with aluminum infiltration from top to bottom, decreasing the capillary force, and the decrease, in turn, causes a decrease in the infiltration rate.

Determining the infiltration rate and time data:

$$v = 0.84773 - 0.02944t + 5.659 \times 10^{-4} t^2 - 4.9524 \times 10^{-6} t^3 + 1.58 \times 10^{-8} t^4 \tag{11}$$
$$(R^2 = 0.99621)$$

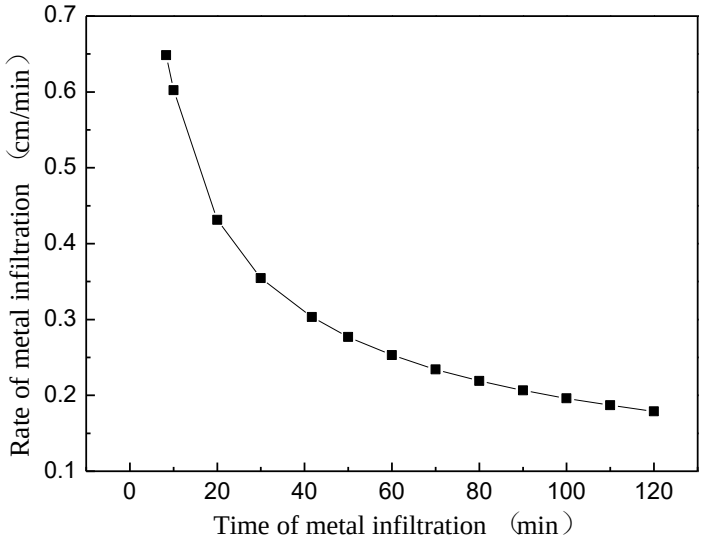


**Figure 4** The relationship between speed and time of infiltration

## Summary

For the first time, the metal infiltration depth and infiltration rate of the BN-Al composite prepared by metal infiltration have been calculated and studied. The calculation results show that the infiltration depth gradually increases with the increase of time, and the final infiltration depth can reach 0.21 m. As time increases and voids decrease, the infiltration rate gradually decreases. The maximum impregnation rate is 0.65cm·min$^{-1}$. This calculation and research provide a positive idea for the calculation and prediction of metal infiltration in void media in future studies.

## Notes

The authors declare that they have no competing financial interest.

## Acknowledgements

This work was supported by the fundamental, scientific-research business resources of the central universities (award # N10060200).

## References

1. C. Wang *et al.*, Research Progress on Aluminum-Boron Compounds (Al-B) and Its Composite Materials. *Bulletin of the Chinese Ceramic Society*, 26 (2013).
2. V. I. Matkovich, *Boron and refractory borides* (Springer, 1977).
3. D. Gosset, M. Guery, B. Kryger (1991) Thermal properties of some boron-rich compounds ("BnC" and $AlB_{12}$). in *AIP Conference Proceedings* (American Institute of Physics), pp 380-383.

4. X. Luo *et al.*, Influence of metallic additives on densification behaviour of hot-pressed $TiB_2$. *Light Metals*, 1151-1155 (2009).
5. X. Cao *et al.* (2011) High temperature electrochemical synthesis of tungsten boride from molten salt. in *Advanced Materials Research* (Trans Tech Publ), pp 463-466.
6. C. Wang, X. Xue, X. Cao, H. Yang, Effect of BN Addition on Mechanical Properties and Microstructure of $TiB_2$-Al Composites. *Journal of Northeastern University (Natural Science)*, 19 (2012).
7. X. Hu *et al.* (2007) $Nd_2O_3$ Solubility in $NdF_3$-LiF-$Nd_2O_3$ Melts. in *Proceedings of NGCWP 2007*.
8. B. R. Golla, A. Mukhopadhyay, B. Basu, S. K. Thimmappa, Review on ultra-high temperature boride ceramics. *Progress in Materials Science* **111**, 100651 (2020).
9. C. Wang *et al.*, A New Method of Fabricating AlN-$TiB_2$ Composite Ceramics. *Materials and manufacturing processes* **28**, 953-956 (2013).
10. C. Wang, J. Zhang, X. X. Xue, X. Z. Cao (2013) Fabrication B-Ni-Al Shielding Materials by Vacuum Metal Infiltration. in *Advanced Materials Research* (Trans Tech Publ), pp 410-413.
11. X. Cao, C. Wang, X. Xue, H. Yang, Preparation of tungsten boride ceramic by pressureless sintering. *Journal of Inorganic Materials* **29**, 498-502 (2014).
12. W. Tao *et al.* (2009) Finite element analysis of thermo-electric coupled field in 400kA large-scale aluminum reduction cell. in *2009 World Non-Grid-Connected Wind Power and Energy Conference* (IEEE), pp 1-4.
13. P. Loganathan, A. Gnanavelbabu, K. Rajkumar, S. Ayyanar (2020) A comparative study of solid lubricant types on the microstructure and mechanical behaviour of AA7075-zirconium boride aerospace composites. in *IOP Conference Series: Materials Science and Engineering* (IOP Publishing), p 012001.
14. C. Wang *et al.*, Research on Thermal Neutron Shielding Performance of $TiB_2$-Al Composite Materials. *ChemRxiv* https://doi.org/10.26434/chemrxiv.13611725.v1 (2021).
15. C. Wang *et al.* (2014) Elementary research on preparation of $AlB_{12}$ powder by self-propagating high-temperature synthesis (SHS). in *Materials Science Forum* (Trans Tech Publ), pp 365-369.
16. X. Cao, C. Wang, X. Xue, G. Cheng, Effect of ti addition on the residual aluminium content and mechanical properties of the $B_4C$-al composites produced by vacuum infiltration. *Archives of Metallurgy and Materials* **60**, 2493-2398 (2015).
17. K. Liang, G. Orange, G. Fantozzi, Evaluation by indentation of fracture toughness of ceramic materials. *Journal of Materials Science* **25**, 207-214 (1990).
18. C. Wang *et al.*, Theoretical Calculation of Self-Propagating High-Temperature Synthesis (SHS) Preparation of $AlB_{12}$. https://doi.org/10.26434/chemrxiv.13591427.v1. (2021).
19. G. E. Gazza, M. W. Lindley (1975) Ceramic-metal systems by infiltration. (Google Patents).
20. X. Cao *et al.*, Electrochemical Behavior and Electrodeposition of Sn Coating from Choline Chloride–Urea Deep Eutectic Solvents. *Coatings* **10**, 1154 (2020).
21. D. Qi *et al.*, Preparation and Erosion Performance for Co-continuous Phase Composites of $Si_3N_4$/1Cr18Ni9Ti. *Chinese Journal of Materials Research* **33**, 34-42 (2019).
22. M. Humenik Jr, N. M. Parikh, Cermets: I, fundamental concepts related to micro-structure and physical properties of cermet systems. *Journal of the American Ceramic Society* **39**, 60-63 (1956).

23. C. Wang *et al.*, Preparation of $AlB_{12}$ Powder by Self-Propagating High-Temperature Synthesis (SHS). https://doi.org/10.26434/chemrxiv.13591313.v1. (2021).
24. J. Huang, S. Daryadel, M. Minary-Jolandan, Low-Cost Manufacturing of Metal–Ceramic Composites through Electrodeposition of Metal into Ceramic Scaffold. *ACS applied materials & interfaces* **11**, 4364-4372 (2019).
25. C. Wang, M. E. Hossain Bhuiyan, S. Moreno, M. Minary-Jolandan, Direct-Write Printing Copper–Nickel (Cu/Ni) Alloy with Controlled Composition from a Single Electrolyte Using Co-Electrodeposition. *ACS Applied Materials & Interfaces* **12**, 18683-18691 (2020).
26. M. Mahmoudi *et al.*, Three-Dimensional Printing of Ceramics through "Carving" a Gel and "Filling in" the Precursor Polymer. *ACS Applied Materials & Interfaces* **12**, 31984-31991 (2020).
27. H. Koide, Y. Someya, T. Yoshida, T. Maruyama, Properties of Ni/YSZ cermet as anode for SOFC. *Solid state ionics* **132**, 253-260 (2000).
28. X. Cao *et al.*, Effect of Ni addition on pressureless sintering of tungsten diboride. *International Journal of Refractory Metals and Hard Materials* **41**, 597-602 (2013).
29. C. Wang, X. Xue, X. Cao, H. Yang, G. Cheng, The effect of Ti addition on the microstructure and fracture toughness of BN-Al composite materials synthesized by vacuum infiltration. *Archives of Metallurgy and Materials* **58**, 509-512 (2013).
30. M. Dong *et al.*, A novel comprehensive utilization of vanadium slag: as gamma ray shielding material. *Journal of hazardous materials* **318**, 751-757 (2016).
31. A. Mortensen, V. J. Michaud, M. C. Flemings, Pressure-infiltration processing of reinforced aluminum. *JOM* **45**, 36-43 (1993).
32. H. Fujii, H. Nakae, K. Okada, Interfacial reaction wetting in the boron nitride/molten aluminum system. *Acta metallurgica et materialia* **41**, 2963-2971 (1993).